

## RESEARCH ARTICLE

10.1002/2015JA021547

## Key Points:

- Receptions in the conjugate hemisphere can be predicted based on the  $K_p$  index from preceding days
- Machine-learning techniques predict conditions for receptions with substantially higher accuracies
- Receptions require a period of higher geomagnetic activity and then quieting at transmission

## Correspondence to:

J. D. Li,  
jdl@stanford.edu

## Citation:

Li, J. D., M. Spasojevic, and U. S. Inan (2015), Predicting conditions for the reception of one-hop signals from the Siple transmitter experiment using the  $K_p$  index, *J. Geophys. Res. Space Physics*, 120, doi:10.1002/2015JA021547.

Received 8 JUN 2015

Accepted 15 SEP 2015

Accepted article online 19 SEP 2015

# Predicting conditions for the reception of one-hop signals from the Siple transmitter experiment using the $K_p$ index

J. D. Li<sup>1</sup>, M. Spasojevic<sup>1</sup>, and U. S. Inan<sup>1,2</sup>
<sup>1</sup>Department of Electrical Engineering, Stanford University, Stanford, California, USA, <sup>2</sup>Department of Electrical Engineering, Koc University, Istanbul, Turkey

**Abstract** Wave injection experiments provide an opportunity to explore and quantify aspects of nonlinear wave-particle phenomena in a controlled manner. Waves are injected into space from ground-based ELF/VLF transmitters, and the modified waves are measured by radio receivers on the ground in the conjugate hemisphere. These experiments are expensive and challenging projects to build and to operate, and the transmitted waves are not always detected in the conjugate region. Even the powerful transmitter located at Siple Station, Antarctica in 1986, estimated to radiate over 1 kW, only reported a reception rate of ~40%, indicating that a significant number of transmissions served no observable scientific purpose and reflecting the difficulty in determining suitable conditions for transmission and reception. Leveraging modern machine-learning classification techniques, we apply two statistical techniques, a Bayes and a support vector machine classifier, to predict the occurrence of detectable one-hop transmissions from Siple data with accuracies on the order of 80%–90%. Applying these classifiers to our 1986 Siple data set, we detect 406 receptions of Siple transmissions which we analyze to generate more robust statistics on nonlinear growth rates, 3 dB/s–270 dB/s, and nonlinear total amplification, 3 dB–41 dB.

## 1. Introduction

Magnetospheric wave injection experiments are an important tool for studying nonlinear wave-particle interactions and the resulting phenomena. One particularly prolific such experiment is the Siple Transmitter Experiment, which operated from 1973 to 1988 [Li *et al.*, 2014] from Siple Station, Antarctica (75.93°S, 84.25°W geographic and  $L = 4.2$ ). This experiment injected ELF/VLF waves into the magnetosphere, where they were modified in interactions with energetic electrons in the radiation belts, and the resulting waves were observed at a receiver located in the conjugate hemisphere at Lake Mistissini, Canada (50.42°N, 73.87°W geographic) for the data analyzed here. (Prior to 1986, the receiver in the conjugate hemisphere was originally located at Roberval, Canada.) The observations of various nonlinear wave-particle interaction phenomena, such as nonlinear amplification and the generation of triggered emissions [Helliwell, 1979, 1988], provided early opportunities to characterize the phenomena and remain an important source of data for validating theoretical analysis and the numerical simulation of wave-particle interactions [Gibby *et al.*, 2008; Hikishima and Omura, 2012; Nunn and Omura, 2012; Li *et al.*, 2015].

The experiment generated a substantial volume of data, but early work typically focused on individual examples and case studies, making generalizations of behavior from anecdote rather than statistics. In the years since the Siple Experiment, significant advances in computational resources allow us to digitize, store, and process large volumes of data in order to rigorously quantify the range of observed nonlinear effects. Recently, the original analog magnetic tapes containing the ground-based ELF/VLF measurements from Siple and the conjugate region receivers have been digitized, containing 6971 h of data. Recent analysis efforts have focused on statistically quantifying nonlinear amplification and the generation of triggered emissions [Li *et al.*, 2014, 2015].

One particular limitation of working with data from the Siple Experiment has been the relatively low rate of reception in the conjugate hemisphere, with only ~40% of Siple transmissions being detected [Gibby, 2008; Li *et al.*, 2015]. In order for Siple signals to be observed in the conjugate hemisphere, they must propagate in the magnetosphere within field-aligned density irregularities known as ducts [Angerami, 1970]. The reception

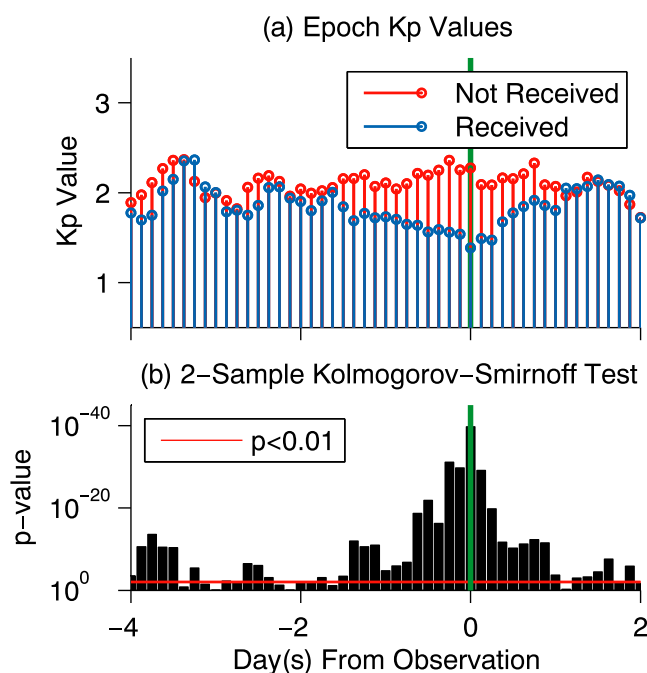


**Figure 1.** (a) Superposed epoch analysis of the mean  $K_p$  index over a 6 day period of minidiagnostic (MDIAG) transmissions detected (blue) and of transmissions not detected (red) at the receiver in the conjugate hemisphere. (b) The  $p$  values for a two-sample Kolmogorov-Smirnov statistical significance test are plotted for each 3 h interval, and the y axis is inverted so that the more significant  $p$  values are better highlighted. This figure is an updated version considering a larger number of transmissions from Figure 4 in Li et al. [2014].

of signals transmitted from Siple is more likely when geomagnetic conditions are less disturbed [Carpenter and Bao, 1983; Li et al., 2014]. This requirement for quieting in  $K_p$  was also observed in wave injection experiments using the HAARP ionospheric heater [Golkowski et al., 2011] and was attributed to the formation of stable ducts. Figure 1a shows a superposed epoch analysis of the  $K_p$  index from 4 days before to 2 days after the time of transmission for Siple transmissions received and not received in the conjugate hemisphere. There is a significant difference, as described by a Kolmogorov-Smirnov significance test as shown in Figure 1b, in the geomagnetic conditions characterized by the  $K_p$  index with a period of quieting beginning several days prior to intervals with successful receptions of transmissions, indicating the potential utility of using the  $K_p$  index to evaluate in advance conditions suitable for the reception of magnetospherically propagating signals. As further described in section 2.1, Figure 1 is generated using the  $K_p$  index behavior associated with 1093 Siple transmissions from 1986, with 423 receptions and 670 nonreceptions observed in the conjugate hemisphere.

The key information that allows for detecting a Siple transmission at the receiver comes from transmission logs which detail the transmission format (the frequency-time elements transmitted in a set sequence), the transmission time, and the  $f_{\text{set}}$  transmission frequency (the central tuning frequency to which transmitted elements were referenced). While the most thorough detection method would be a visual inspection of spectrograms of data from the conjugate region and manual detection of receptions, this manual identification process does not scale with the amount of data and becomes too time consuming as the amount of data increases. Another method attempts to automatically detect signals using a signal amplitude threshold that determines if a sufficiently strong signal is above the noise floor [Li et al., 2014], but this approach suffers from inherent limitations in only detecting strongly amplified signals in the presence of low background noise conditions and is not sufficiently robust. Here we demonstrate the application of machine-learning classification techniques as a preprocessing step for selecting intervals when receptions may be significantly more likely. There has been thus far limited work in the space physics community taking advantage of more recent machine-learning techniques, and most such results, using, for instance, support vector machines, tend to be for regression models [Gavrishchaka and Ganguli, 2001; Ji et al., 2013; Yue et al., 2015].

Given the significant difference in the  $K_p$  index between received and not received Siple transmissions, we apply two methods for classifying transmissions to develop a model for predicting intervals of receptions of

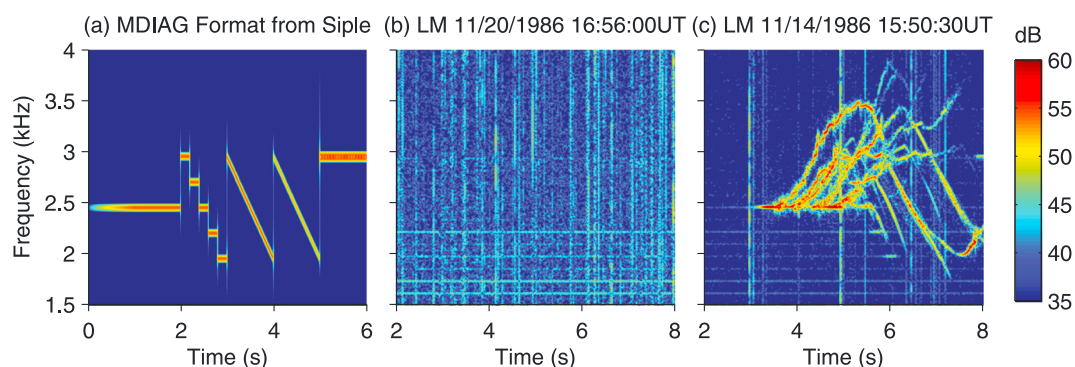


**Figure 2.** (a) Illustration of the MDIAG transmission format transmitted from Siple Station and conjugate observations at Lake Mistissini (LM) showing examples of a case where (b) the transmission was not received and (c) the transmission was received.

Siple transmissions at Lake Mistissini based on the geomagnetic  $Kp$  index from the 6 days preceding the time of transmission. Both methods, a naive Bayes classifier with Laplace smoothing and a support vector machine classifier, have prediction accuracies of 80%–90%. We also demonstrate the statistical advantages of these classification approaches by using the detected cases to update the statistics on nonlinear growth rate and total growth of injected signals first presented in *Li et al.* [2014]. Applying these classifier approaches, using the  $Kp$  index, to experimental studies may allow for more efficient experiments by selecting transmission times and conditions that are significantly more likely to result in reception, and these techniques may provide insight into understanding the conditions that lead to wave amplification from wave-particle interactions.

## 2. Classification Methodologies

Although there are many different classification techniques, we consider two simple supervised learning methods for classification, naive Bayes with Laplace smoothing and support vector machines. We first describe the common data set used for both classification approaches, including the generation of the ground truth labels describing signal reception and the  $Kp$  geomagnetic indices used as the input feature set, and then provide some intuition regarding the two classification techniques. While a naive Bayes classifier is a commonly first implemented classifier to determine the effectiveness of applying machine-learning techniques, a support vector machine (SVM) classifier is a more sophisticated and computationally intensive method that often yields more accurate predictions although its internal parameters are more opaque.

### 2.1. The MDIAG Data Set

The data set is composed of observations of transmissions of a minidiagnostic (MDIAG) format during 1986. This builds on the data set first developed by *Li et al.* [2014] in focusing on this single-transmission format transmitted by Siple from April to December of 1986 and observed at the conjugate receiver at Lake Mistissini (LM). The MDIAG format was a frequently transmitted format with a variety of elements used to evaluate the conditions for transmitting different subsequent formats and is illustrated in Figure 2a. The format begins with a 2 s tone at the central tuning frequency,  $f_{\text{set}}$  (with an amplitude ramp from  $-10$  dB to  $0$  dB over the first second), followed by a descending staircase of five 200 ms tones spaced 250 Hz apart from  $f_{\text{set}} + 500$  to  $f_{\text{set}} - 500$ , two descending frequency ramps (the first at  $0$  dB and the second at  $-6$  dB) over the same frequency range for 1 s each, and a 7 s long pair of constant frequency tones (called a doublet) at  $f_{\text{set}} + 480$  and at  $f_{\text{set}} + 510$  at  $0$  dB. These elements can be visually identified on spectrograms in order to determine if the transmission was received in the conjugate hemisphere.

In 1986, we have data for 1093 transmissions of the MDIAG format, and as shown in Figure 2b, not all transmissions were received and detected at Lake Mistissini. To develop ground truth labels describing the detection of receptions of MDIAG transmissions, we process each MDIAG case into high frequency and time resolution spectrograms and manually determine if the MDIAG transmission is observed through a visual inspection of the spectrogram, as in Figure 2c. Of the 1093 transmissions, 423 receptions were detected and 670 were not detected, giving a 39% reception rate. This matches well with general statistics compiled by *Gibby* [2008] and with the smaller number of transmissions of a different format studied in *Li et al.* [2015]. We label the received transmissions as Class 1 and the not received transmissions as Class 0.

We select the  $Kp$  index as the input feature for the classification methods, in particular, the  $Kp$  index from the 6 days preceding the time of transmission and including the  $Kp$  index at transmission. The  $Kp$  index was chosen by noting that receptions generally occur when the geomagnetic condition as described by  $Kp$  is less disturbed [Carpenter and Bao, 1983] and that geomagnetic conditions described by the  $Kp$  index differ between cases of reception and nonreception [Li et al., 2014]. The 6 days preceding the time of transmission were selected to include the entire window of time originally chosen for conducting the epoch analysis of  $Kp$  behavior for received and not received cases shown in Figure 1a. An analysis of the significant intervals from Figure 1b may indicate that fewer days may suffice as well.

## 2.2. Naive Bayes With Laplace Smoothing

The naive Bayes classifier belongs to the class of generative learning algorithms that model the distributions of the input features for each class that the algorithm is trying to learn. Generative learning algorithms are a supervised learning approach, which requires the training data to first be manually labeled. By assuming that the features are conditionally independent given the class, the resulting algorithm is the well-understood naive Bayes classifier [Rish, 2001]. In practice, the naive Bayes classifier works by first training the conditional probability of each feature given each class. This corresponds with maximizing the likelihood of a given class occurring given a set of features. Then, using the conditional probabilities trained for each feature, new cases can be evaluated by calculating the conditional probability for each class and assigning a label for the class that is more likely. Laplace smoothing adds a small, but nonzero probability to the conditional probabilities for all of the features in order to prevent results with an indeterminate form; that is, both the numerator and denominator are 0. This extends the functionality of the classifier to generate predictions for cases with new features that were not identified in training. In the work presented here, the class labels are “1” for received transmissions and “0” for not received transmissions. As the  $Kp$  index can vary substantially and the quieting may be the important characteristic indicating suitable ducting conditions for propagation, we instead used the change in  $Kp$  between 3 h intervals as the input feature for the naive Bayes classifier. Furthermore, as the input features to these Bayes classifiers must be binary valued, we implement a simple binary representation by creating a large lookup table binary array.

## 2.3. Support Vector Machines

Support vector machines were developed by Cortes and Vapnik [1995] and have become a widely used algorithm in the machine-learning community. SVMs can be conceptualized as a way of separating the data by its features into distinct classes by projecting the data into a higher dimensional space where the classes can then be separated by a hyperplane. The projection depends on the chosen mathematical transformation, called a kernel, and the hyperplane maximizes the distance to the closest points. The set of the closest points to the hyperplane are then called support vectors. As the kernel transformation of the input features for the hyperplane separation is more opaque to understanding the specific workings of the classifier and as the input features do not need to be binary valued, here we use the  $Kp$  indices directly as the input data features. We implement this SVM classifier utilizing a standard, off-the-shelf implementation called LibSVM by Chang and Lin [2011].

## 3. Classification Results

We apply these two classification techniques to the MDIAG data set, using the  $Kp$  indices from the 6 days preceding the time of transmission to automatically predict whether or not the MDIAG transmission is detected. First, we train the naive Bayes classifier feature weights and the support vector machine classifier model on a training set composed of 810 transmissions, with 317 detections and 493 undetected cases so that the training set distribution of detected and undetected cases is reflective of the overall reception rates in the data. Then, we evaluate the accuracy of the models and verify their validity by analyzing their predictions given a new set of testing data, the remaining 283 cases, with 106 detections and 177 undetected cases, which were never used in the training of the models. For the amount of data considered here, both models take a negligible amount of time to train and to generate predictions. The detected and undetected cases used in the training and testing sets were randomly selected from the entire set of data, and the classification results are broadly applicable as validated through repeated random subsampling validation.

The prediction results and how they compare with the ground truth labels are shown in a confusion matrix in Table 1. The upper half describes the results for the Bayes classifier, and the lower half for the SVM classifier. The left column describes results for the training data, and the right column the results for the testing data.

**Table 1.** Confusion Matrix Showing the Prediction Results of MDIAG Reception and Nonreception for the Bayes and SVM Classifiers<sup>a</sup>

	Observations of MDIAG Transmissions					
	Training			Testing		
	Total	Received	Not Received	Total	Received	Not Received
	810	317	493	283	106	177
Bayes predicted						
Received	301	270	31	111	92	19
Not received	509	47	462	172	14	158
SVM predicted						
Received	300	278	22	115	97	18
Not received	510	39	471	168	9	159

<sup>a</sup>The confusion matrix describes the number of true and false positives and negatives for each classifier.

The numbers indicate the predicted or observed number of transmissions. Overall, the accuracy for the Bayes classifier is 90% (732/810) for the training data and 88% (250/283) for the test data. The accuracy is representative of the predictive capability of the classifier, with a high precision (correctly predicted detections divided by all predicted detections) of 90% and of 83% and a high recall (correctly predicted detections divided by all detections) of 85% and 87% for the training and test data, respectively. The results for the SVM are similar, if not slightly better. The accuracy is 92% and 90%, the precision is 93% and 84%, and the recall is 88% and 92% for the training and test data, respectively. Incorrectly classified cases reveal transmissions where the *Kp* behavior of received cases more closely resembles the *Kp* behavior of nonreception transmissions, and a visual examination of the transmissions shows that these receptions are also usually weaker and less active.

Both classifiers perform well, with 80% to 90% accuracies in predicting the reception and nonreceptions of transmitted Siple MDIAG signals. This compares favorably with the actual reception statistics, where the transmissions were detected only 40% of the time and may prove useful for guiding the operations of future wave injection experiments or further analysis of the historic Siple data set. As *Kp* is a global geomagnetic index with a 3 h resolution, efforts were made to consider the potential improvement in prediction by using local magnetometer stations and by using a geomagnetic index with higher time resolution. However, using data from three Canadian *K* indices stations, at Meanook, Ottawa, and Victoria, as the input features for both the Bayes and SVM classifiers did not improve the prediction accuracies. Similarly, using the 1 min *AE* index as the input feature to improve the time resolution was not successful, as the higher time resolution resulted in too large of an input feature set, leading to overfitting and to ill-suited classifiers. Nonetheless, training the classifiers on finer time resolution index values, which requires a larger number of training cases to avoid the issues of overfitting, can improve the accuracy of these classifiers. Figure 6 of Sonwalkar *et al.* [1997] demonstrates that the reception occurrence rate can vary over the scale of minutes, and errors in our predictions can be attributed to these variations in the reception rate. The current 3 h resolution, while likely capturing the relevant overall magnetospheric conditions necessary for reception, should be improved at least to 30 min or hour-long resolutions to more accurately describe the reception conditions.

Having demonstrated the predictive capability of these two machine-learning techniques, we also provide a general understanding of when these classifiers can be utilized effectively. Figure 3 illustrates the learning curve for the SVM predictor (or classifier), describing the training (blue) and testing (red) accuracy as a function of the number of training cases. Note that the training accuracy is generally high, over 90%, regardless of the number of training cases. This is due to the mechanics of the SVM predictor, which tends to classify the training data with high accuracy. To evaluate if the classifier has reasonable accuracy, it is more important to consider the testing prediction accuracy and determine when it is comparable with the training accuracy. Here we see that when the classifier is trained on more than 250 training cases, the testing prediction accuracy exceeds 85% consistently, in spite of some oscillations due to the random sampling method employed. Having demonstrated the power and broad applicability of machine-learning techniques to data of varying sample sizes, in particular, using the SVM classifier/predictor, we point out that utilizing more data tends to increase the prediction accuracy and also that the training data must have a balanced composition of the different classes of data in order to generate meaningful predictions.

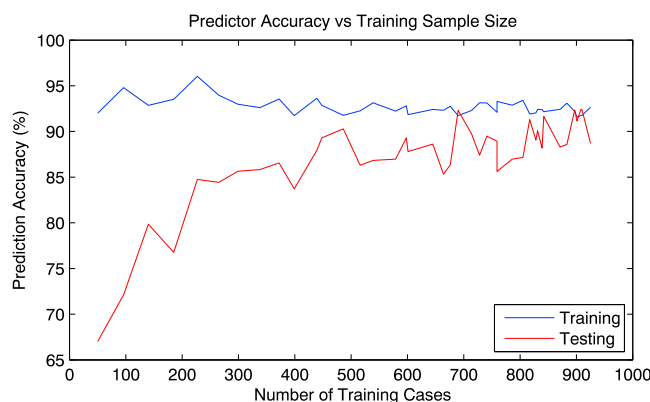


**Figure 3.** A learning curve for the SVM classifier illustrating the prediction accuracy for the training (blue) and testing (red) data as a function of the number of training cases utilized. The oscillations in the learning curve are due to the random sampling of the data for training and testing.

While the SVM classifier tends to be more accurate, it also is opaque to understanding the structure of the hyperplane (i.e., the boundary in the higher dimensional feature space that separates the two classes in the data) and how the data is classified. Here we can instead consider the structure of the Bayes classifier. The Bayes classifier generates probabilities for each element in the feature set, and an examination of these probabilities may indicate additional details. Some precision in interpreting these results are required though, as each element in the feature set describes a given change in  $K_p$  index between intervals for a given day preceding transmission. We find that the most predictive element, indicating that reception is 42 times more likely, is the token describing an increase in  $K_p$  index of two units during the interval of 3 days before the time of transmission. This is interesting in pointing out that not only is the overall quieting needed for the formation of a stable duct for wave propagation but also a prior interval of higher geomagnetic activity, presumably associated with the injection of energetic electrons into the inner magnetosphere, is also key to driving the wave amplification such that reception of signals in the conjugate region is possible.

#### 4. Updated Siple Statistics

Using the large number of detected MDIAG transmissions, we can provide updated statistics on nonlinear amplification characteristics following the work of *Li et al.* [2014]. Here we have significantly more cases, 407 instead of 106, and we apply the same analytical approach in order to extract the amplitude characteristics that describe the amplification behavior of injected whistler mode signals using the 2 s long tone transmitted at the beginning of the MDIAG format. As before, we first extract 4 s of the full broadband data covering 2 s of noise and the 2 s long tone and remove the noise from lightning-generated impulses, as shown in Figure 4a. To find the narrowband signal amplitude, we multiply the broadband data by a complex exponential, shifting the signal from its  $f_{\text{set}}$  transmission frequency to baseband and filtering out other noise with a 100 Hz low-pass filter. Finally, we smooth with a 10-point median filter to reduce impulsive noise in the signal and normalize using the closest preceding reference calibration tone. From the narrowband signal amplitudes for all 407 cases, we measure the noise floor, the saturation power level, and the nonlinear growth rate as illustrated in Figure 4b. In this characteristic amplitude plot, the noise floor (dashed red line) is interrupted by the signal growing out of the noise at a nonlinear growth rate (dashed orange line), here 159.5 dB/s, and the signal amplifies until saturating at the saturation threshold (dashed green line).

The use of these larger number of MDIAG transmissions provides an improved statistical understanding of wave amplification behavior of injected whistler mode waves, as presented in Figures 4c–4e. This improves on the results presented in *Li et al.* [2014] and even more so on statistics from earlier work such as *Helliwell and Katsufakis* [1974] and *Helliwell et al.* [1980]. Figure 4c shows a histogram of the nonlinear growth rates, which ranges from 3 dB/s to 270 dB/s with a median growth rate of 68 dB/s. These values cover the range of 30–200 dB/s observed by *Helliwell et al.* [1980] and provides a better understanding of the distribution of the growth rates. Figure 4d shows a histogram of total nonlinear growth, calculated as the difference between the saturation threshold and the noise floor, which ranges from 3 dB to 41 dB with a median total growth of 18 dB. While these total growths, as mentioned in *Li et al.* [2014] cover the ranges observed in

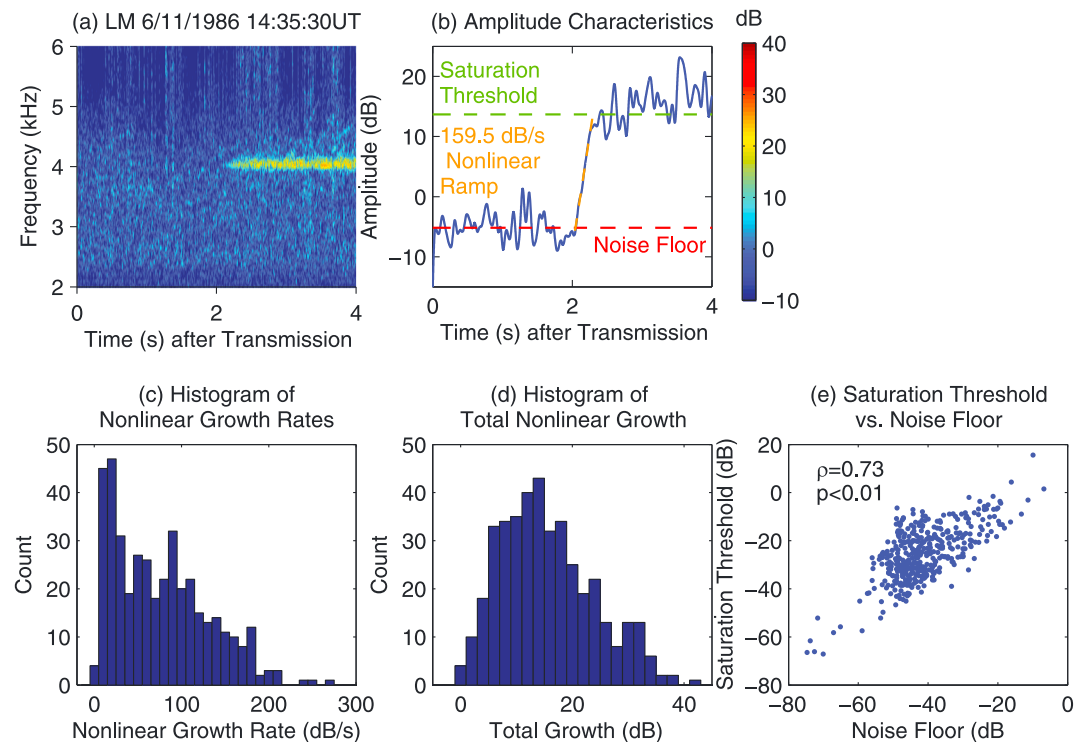


**Figure 4.** (a) Example spectrogram of the long-tone element in an MDIAG transmission from Siple Station. (b) The narrowband amplitude of the long tone is characteristic of most observations where the signal amplifies out of the noise floor (dashed red line), undergoing nonlinear amplification (dashed orange line) until saturating (dashed green line). Statistics compiled from the amplitude characteristics of all MDIAG transmissions are presented as (c) a histogram of the observed nonlinear growth rates, (d) a histogram of the observed total nonlinear growth, and (e) a scatterplot of the saturation power level versus the noise floor ( $\rho = 0.73$ ,  $p < 0.01$ ).

Helliwell and Katsufrakis [1974], we again see that the often-cited 30 dB value of expected total growth should be adjusted to around 20 dB. Although these values are most directly applicable to 1986, these bounds provide improved statistical justification that may apply more generally. Finally, Figure 4e shows a significant correlation ( $\rho = 0.73$ ,  $p < 0.01$ ) between the saturation threshold and the noise floor. The correlation here improves upon, in significance and correlation, the earlier observation in Li *et al.* [2014] and supports the hypothesis that conditions favoring higher linear amplification drive higher noise floors and also higher maximum amplification thresholds for transmitted signals. Note that this statistical analysis of the signals tends to aggregate transmissions under potentially widely varying amplification conditions. Finer time resolution analysis would allow for identification of the hour- and minute-scale temporal variations in occurrence rate and in amplification effects as measured by the saturation threshold and the nonlinear growth rates as observed in Sonwalkar *et al.* [1997].

## 5. Conclusions

As the scale of data increases and scope of experiments include many more cases, more sophisticated techniques for detection or classification may become more useful. Looking at a set of experiments from the Siple transmitter experiment in 1986, we demonstrate the application of a naive Bayes with Laplace smoothing classifier and a support vector machine classifier for the automatic detection of transmitted MDIAG transmissions received at the conjugate receiver at Lake Mistissini. This is a nontrivial problem with 1093 transmissions that are received at a 39% reception rate for a total of 423 receptions. The classifiers take as input features the  $K_p$  indices from the preceding 6 days to predict the reception of transmissions with 80%–90% accuracy. This work suggests further utilization of machine-learning techniques for active experiments in maximizing the number of detectable receptions for scientific analysis, especially with the higher accuracies afforded by more sophisticated techniques such as the SVM classifier. By analyzing the Bayes classifier probabilities, we find that the most predictive token is a period of increasing activity 3 days prior to transmission. Thus, we

conclude that reception of Siple signals requires a period of higher geomagnetic activity, which results in higher fluxes of energetic electrons for wave amplification, followed by a period of quieting, which results in the formation of stable-ducted paths for wave propagation.

The larger number of detected transmissions can also be used to improve our statistical understanding of wave amplification behavior in studying the modifications of injected whistler mode waves by wave-particle interactions. Here 407 of the transmissions include the 2 s long tone from which we can measure the noise floor, the nonlinear growth rate, and the saturation threshold of the narrowband signal amplitude. The nonlinear growth rates range from 3 dB/s to 270 dB/s, and the total nonlinear growth ranges from 3 dB to 41 dB with a median growth of 18 dB. And a significant correlation between the saturation threshold and the noise floor confirms the result in *Li et al.* [2014].

## Acknowledgments

This work is supported by AFRL award FA9453-11-C-0011 to Stanford University. We are grateful to Vijay Harid, Timothy Bell, and Donald Carpenter for helpful discussions. Requests for the data used for analysis can be directed to the corresponding author.

Michael Balikhin thanks Vikas Sonwalkar and Andrew Gibby for their assistance in evaluating this paper.

## References

- Angerami, J. J. (1970), Whistler duct properties deduced from VLF observations made with the OGO 3 satellite near the magnetic equator, *J. Geophys. Res.*, *75*, 6115–6135, doi:10.1029/JA075i031p06115.
- Carpenter, D. L., and Z. T. Bao (1983), Occurrence properties of ducted whistler-mode signals from the new VLF transmitter at Siple Station, Antarctica, *J. Geophys. Res.*, *88*, 7051–7057, doi:10.1029/JA088iA09p07051.
- Chang, C.-C., and C.-J. Lin (2011), (LIBSVM): A library for support vector machines, *ACM Trans. Intel. Syst. Technol.*, *2*(3), 27:1–27:27.
- Cortes, C., and V. Vapnik (1995), Support-vector networks, *Mach. Learn.*, *20*(3), 273–297.
- Gavrishchaka, V. V., and S. B. Ganguli (2001), Support vector machine as an efficient tool for high-dimensional data processing: Application to substorm forecasting, *J. Geophys. Res.*, *106*(A12), 29,911–29,914, doi:10.1029/2001JA900118.
- Gibby, A. R. (2008), Saturation effects in VLF triggered emissions, Stanford Univ., Stanford, Calif.
- Gibby, A. R., U. S. Inan, and T. F. Bell (2008), Saturation effects in the VLF-triggered emission process, *J. Geophys. Res.*, *113*, A11215, doi:10.1029/2008JA013233.
- Golkowski, M., M. B. Cohen, D. L. Carpenter, and U. S. Inan (2011), On the occurrence of ground observations of ELF/VLF magnetospheric amplification induced by the HAARP facility, *J. Geophys. Res.*, *116*, A04208, doi:10.1029/2010JA016261.
- Helliwell, R. A. (1979), Siple station experiments on wave-particle interactions in the magnetosphere, in *Wave Instabilities in Space Plasmas; Proceedings of the Symposium, Helsinki, Finland, July 31–August 8, 1978*, edited by P. J. Palmadesso and K. Papadopoulos, pp. 191–203, D. Reidel, Dordrecht, Netherlands.
- Helliwell, R. A. (1988), VLF wave-injection experiments from Siple Station, Antarctica, *Adv. Space Res.*, *8*, 279–289, doi:10.1016/0273-1177(88)90373-0.
- Helliwell, R. A., and J. P. Katsufakis (1974), VLF wave injection into the magnetosphere from Siple Station, Antarctica, *J. Geophys. Res.*, *79*(16), 2511–2518, doi:10.1029/JA079i016p02511.
- Helliwell, R. A., D. L. Carpenter, and T. R. Miller (1980), Power threshold for growth of coherent VLF signals in the magnetosphere, *J. Geophys. Res.*, *85*, 3360–3366, doi:10.1029/JA085iA07p03360.
- Hikishima, M., and Y. Omura (2012), Particle simulations of whistler-mode rising-tone emissions triggered by waves with different amplitudes, *J. Geophys. Res.*, *117*, A04226, doi:10.1029/2011JA017428.
- Ji, E.-Y., Y.-J. Moon, J. Park, J.-Y. Lee, and D.-H. Lee (2013), Comparison of neural network and support vector machine methods for Kp forecasting, *J. Geophys. Res. Space Physics*, *118*, 5109–5117, doi:10.1002/jgra.50500.
- Li, J. D., M. Spasojevic, V. Harid, M. B. Cohen, M. Golkowski, and U. S. Inan (2014), Analysis of magnetospheric ELF/VLF wave amplification from the Siple Transmitter experiment, *J. Geophys. Res. Space Physics*, *119*, 1837–1850, doi:10.1002/2013JA019513.
- Li, J. D., V. Harid, M. Spasojevic, M. Golkowski, and U. S. Inan (2015), Preferential amplification of rising versus falling frequency whistler mode signals, *Geophys. Res. Lett.*, *42*, 207–214, doi:10.1002/2014GL062359.
- Nunn, D., and Y. Omura (2012), A computational and theoretical analysis of falling frequency VLF emissions, *J. Geophys. Res.*, *117*, A08228, doi:10.1029/2012JA017557.
- Rish, I. (2001), An empirical study of the naive Bayes classifier, in *IJCAI 2001 Workshop on Empirical Methods in Artificial Intelligence*, vol. 3, pp. 41–46, IBM, New York.
- Sonwalkar, V. S., D. L. Carpenter, R. A. Helliwell, M. Walt, U. S. Inan, D. L. Caudle, and M. Ikeda (1997), Properties of the magnetospheric hot plasma distribution deduced from whistler mode wave injection at 2400 Hz: Ground-based detection of azimuthal structure in magnetospheric hot plasmas, *J. Geophys. Res.*, *102*, 14,363–14,380, doi:10.1029/96JA03047.
- Yue, C., C.-P. Wang, L. Lyons, Y. Wang, T.-S. Hsu, M. Henderson, V. Angelopoulos, A. T. Y. Lui, and T. Nagai (2015), A 2-D empirical plasma sheet pressure model for substorm growth phase using the support vector regression machine, *J. Geophys. Res. Space Physics*, *120*, 1957–1973, doi:10.1002/2014JA020787.